SPE-193879-MS

A General Framework Model for Fully Coupled Thermal-Hydraulic-Mechanical Simulation of CO2 EOR Operations

Shihao Wang, Colorado School of Mines; Yuan Di, Peking University; Yu-Shu Wu and Philip Winterfeld, Colorado School of Mines

This paper was prepared for presentation at the SPE Reservoir Simulation Conference held in Galveston, Texas, USA, 10–11 April 2019.

Abstract

In this work, we present the development of a comprehensive mathematical formulation and reservoir simulator for thermal-hydraulic-mechanical simulation of CO_2-EOR processes

We adopt the integral finite difference method to simulate coupled thermal-hydraulic-mechanical processes during CO2-EOR in conventional and unconventional reservoirs. In our method, the governing equations of the multiphysical processes are solved fully coupled on the same unstructured grid. A multiscale algebraic linear solver is adopted to speed up the non-isothermal flow calculation. Inspired by the meshless method, the algebraic solver eliminates the low-frequency terms through smoothing on a coarse grid. In order to simulate the phase behavior of a three-phase system, a three-phase flash calculation module, based on direct minimization of Gibbs energy, is implemented in the simulator.

We have investigated the impact of cold CO_2 injection on injectivity as well as on phase behavior. We conclude that cold injection is an effective way to increase injectivity in tight-oil reservoirs. We have observed and studied the temperature decreasing phenomena near the production well, known as the Joule-Thomson effect, induced by expansion of in-situ fluids.

The novelty of this work lies in the fully coupled simulation scheme, including non-isothermal effects on CO2-EOR processes and recoveries, which has been ignored in almost all modeling studies of CO2-EOR. The multiscale solution strategy and the unique phenomena of non-isothermal compositional modeling coupled with geomechanics are captured by our simulator.

Introduction

CO_2 flooding is a proven and promising EOR technique for tertiary recovery. The injected CO_2 has a variety of impacts on the in-situ oil-water system, including the expansion of oil volume and the reduction of oil viscosity as well as capillary forces (Grigg and Schechter 1997). During the past three decades, the number of active CO_2 flooding projects in the United States has increased by more than 300% (Manrique et al. 2010). CO_2 flooding has brought many water-flooded reservoirs back to life by increasing the recovery factor by up to 30%, as summarized in (Rao 2001). For immiscible CO_2 flooding, CO_2 usually turns into a supercritical phase in the high-pressure high-temperature downhole environment. The density of injected

supercritical CO_2 is usually lighter than that of the in-situ hydrocarbons. Therefore supercritical CO_2 may override oil. Meanwhile, as the viscosity of injection CO_2 is much smaller than that of the oil phase, viscous fingering and channeling are likely to occur in immiscible CO_2 flooded reservoirs. Although CO2-EOR has achieved huge success in conventional reservoirs, it faces difficulties in applying to unconventional reservoirs. This is primarily because that the extremely low permeability of unconventional reservoirs limits the injectivity of CO_2.

According to the mechanism of the thermal unloading process (Tang et al. 2019), when cold liquids are injected into the reservoir, the injectivity of the injector should increase. In practice the injectivity increase phenomena near the cold water injector have been widely observed in geothermal reservoirs (Kaya et al. 2011; Stefansson 1997). Such phenomena could be explained by the shrinkage of rock induced by change of thermal stress field (thermal uploading). Especially, in the fractured geothermal reservoir, the injected cold water causes the matrix rock to shrink, increasing the fracture aperture. As the fracture permeability is approximately the cubic power of the fracture aperture, the increase of fracture permeability could be considerable. In this work, we propose to investigate the thermal impact of CO_2 injectivity by conducting a fully coupled thermal-hydraulic-mechanical simulation of CO2-EOR. We have developed a 3D non-isothermal compositional simulator, named MSFLOW_CO2. MSFLOW_CO2 is fully implicit. It solves the thermal-hydraulic-mechanical (THM) in a fully coupled manner, guaranteeing the best numerical stability and the most accurate mass/energy conservation.

To accurately simulate the CO_2-hydrocarbon-water system in the CO_2 flooded reservoir, compositional modeling with flash calculation is needed. The compositional simulator tracks the migration of each component. Within each iteration step, the compositional simulator conducts flash calculation to predict the phase behavior of the system. The flash calculation outputs the phase combination as well as the concentration distribution at a given temperature and pressure. The first trail of flash calculation and compositional modeling for two-phase system dates back to the 1960s (Hoffman 1968). The flash calculation approach brought out by Michelsen (1982a, 1982b) has been widely adopted. Michelsen's approach has two steps. It firstly conducts phase stability test to determine whether a phase exists. It then solves the Rachford-Rice equations (Leibovici and Neoschil, 1992, 1995; Okuno et al. 2010a) using Newton iteration based on the equilibrium ratio (K-value) of each component. Although Michelsen's method has been successfully used in two-phase flash calculation, it has several drawbacks which cause it difficult to be applied to the three-phase flash calculation. Firstly, Michelsen's method has convergence issues, due to the discontinuity of the Rachford-Rice equation. Secondly, Michelsen's method requires multiple iterations and complex phase stability calculation

Recently, Okuno (2010b, 2010c) brought out a reduced model for multiphase flash calculation. Although the reduced model is more efficient compared to traditional K-value approach, its input parameters are relatively hard to be determined. Moreover, the reduced model is only faster than the classic K-value method when the number of components is above 15 to 20, where is not the usual cases for real applications. K-value based flash calculation has been widely adopted in the simulation of CO2-EOR by research code (Pan and Oldenburg 2016) and commercial simulators (Computer Modelling Group LTD. 2010; Schlumberger 2009). In practice, people adopt a 'hybrid' framework for K- value based flash calculation, in which Newton's method is combined with the bi-section method. When Newton's method fails to converge, the algorithm switches to the bi-section method to search for the solution.

Besides the K-value approach, direct minimization of the Gibbs energy is another attractive approach for flash calculation. Direct minimization of the Gibbs energy approach is based on the fact that at the equilibrium state, the Gibbs energy of the system is at its minimum. In the direct minimization of the Gibbs energy approach, the objective function is the total Gibbs free energy of the system. By iteratively tuning the concentration distribution, the approach searches the global minima of the objective function with Newton's method. Therefore, the flash calculation becomes an optimization problem and global

optimization techniques, such as Branch and Bound method (Cheung et al. 2002), tunneling (Nichita et al. 2002), linear programming (Rossi et al. 2009) and heuristic algorithm (Bhargava et al. 2013; Bonilla-Petriciolet and Segovia-Hernández 2010; Walton et al. 2011), can be used to globalize the optimization process. Zhang et al. (2011) have thoroughly reviewed the global optimization techniques for the direct minimization of the Gibbs energy method.

Compared to the K-value approach, the direct minimization of the Gibbs energy method can be more easily applied to multiphase systems. Moreover, this approach is also suitable for the calculation of phase behavior in unconventional reservoirs, in which the capillary pressure has larger impact on the phase equilibrium. To account for the capillary pressure impact, the direct minimization of the Gibbs energy approach adds a surface energy term in its formulation (Rossi et al. 2009). Therefore, this approach has the flexibility to handle the capillary pressure impact in a three-phase system, in which capillary exist both in the gas-liquid phase interface and the liquid-water interface. Recently, Ma (Ma, 2013) adopts a similar approach to investigate the capillary pressure impact on PV-flash by minimizing Helmholtz free energy.

To further improve the speed of the flash calculation, we have also implemented a deep- learning (DL) based proxy flash calculation module. With the breakthrough in both algorithm and hardware, deep learning technology (LeCun et al. 2015) is fast arising. There are already some trails in using DL technology to speed up flash calculation (Al-Marhoun and Osman 2002; Gaganis and Varotsis 2012; Gharbi and Elsharkawy 1997; Zhong et al. 2017). In this work, the proxy flash calculation is based on fully connected networks. It is of accuracy that is up to 97% and is used to replace the physical flash calculation in our compositional simulator MSFLOW_CO2. Our results show that the DL based proxy flash calculation significantly reduces the number of iterations of the flash calculation, and thus speeds up the modeling of CO_2-EOR.

This paper is organized as follows. In Chapter 2 and Chapter 3 we present the flash calculation and equation of state model, respectively. In Chapter 4 and Chapter 5, we discuss the governing equation and mechanical property calculation module for the THM coupling. In Chapter 6, we validate the flash calculation module. In Chapter 7, we present the algorithm and structure of the DL based proxy flash calculation. In Chapter 8, we show a reservoir scale cold CO_2 injection case. The paper is concluded by the discussions in Chapter 9.

Flash calculation

In this session, we present the phase equilibrium (flash) calculation module of MSFLOW_CO2. The purpose of conducting flash calculation is to obtain the phase combination as well as the component distribution of the CO_2-hydrocarbon-water system.

According to thermodynamic principals, at the equilibrium state the Gibbs free energy of the system should be minimized, if the surface energy induced by capillary forces is ignored. The flash calculation in MSFLOW_CO2 is based on the direct minimization of Gibbs energy, following the work of Ballard (Ballard and Sloan 2004; Ballard 2002) and Di et al. (2015)

The Gibbs free energy of a multicomponent system is as follows

$$G = \sum_{\beta=1}^{N_P} \sum_{i=1}^{N_C} n_{i\beta} \mu_{i\beta} \qquad 1$$

In the above equation, $\mu_{i\beta}$ is the chemical potential of component i in phase β. $n_{i\beta}$ is the number of moles of component i in phase β. N_P is the number of phases and N_C is the number of components. In this study, N_P =3. In every flash calculation, we need to define a reference phase r and assume that phase r always exits in the system (If a reference phase disappears, then an alternative phase will be chosen as the reference phase). By introducing the reference phase, we can rearrange Equation *1* as

$$G = \sum_{\beta=1}^{N_P}\sum_{i=1}^{N_C} n_{i\beta}\mu_{ir} + \sum_{\substack{\beta=1\\ \beta\neq r}}^{N_P}\sum_{i=1}^{N_C} n_{i\beta}(\mu_{i\beta} - \mu_{ir}) \quad 2$$

Meanwhile, the fraction of phase β among all the phases is calculated as

$$\alpha_\beta = \sum_{i=1}^{N_C} n_{i\beta}/N_t \quad \beta = 1,\ldots,N_P;\beta \neq r \quad 3$$

In the above equation, N_t is the total number of moles in the whole system, as follows

$$N_t = \sum_{i=1}^{N_C}\sum_{\beta=1}^{N_P} n_{i\beta} \quad 4$$

The mole fraction of the reference phase is

$$\alpha_r = 1 - \sum_{\substack{\beta=1\\ \beta\neq r}}^{N_P} \alpha_\beta \quad 5$$

We then define the Lagrange function and the Lagrange multipliers as follows

$$G^* = G + \sum_{\substack{\beta=1\\ \beta\neq r}}^{N_P} \lambda_\beta(\alpha_\beta - \sum_{i=1}^{N_C} n_{i\beta}/N_t) \quad 6$$

To achieve the minimum Gibbs free energy, the derivative of the above function with respect to all variables should be zero, as

$$\frac{\partial G^*}{\partial n_{i\beta}} = 0, i = 1,\ldots,N_C;\beta = 1,\ldots,N_P;\beta \neq r \quad 7$$

$$\frac{\partial G^*}{\partial \lambda_\beta} = 0, \beta = 1,\ldots,N_P;\beta \neq r \quad 8$$

$$\frac{\partial G^*}{\partial \alpha_\beta} = \lambda_\beta, \beta = 1,\ldots,N_P;\beta \neq r \quad 9$$

According to the above equations, when phase β exists ($\alpha_k > 0$), λ_β should be 0. Therefore, the condition for phase β to exist is

$$\alpha_\beta\lambda_\beta = 0, \beta = 1,\ldots N_P;\beta \neq r \quad 10$$

Moreover, it can be solved that

$$\lambda_\beta/N_t = \mu_{i\beta} - \mu_{ir} = RT\ln(f_{i\beta}/f_{ir}) \quad i = 1,\ldots,N_C;\beta = 1,\ldots,\pi;\beta \neq r \quad 11$$

Where $f_{i\beta}$ and f_{ir} is the fugacity of component i in an arbitrary phase β and the reference phase r respectively.

$$\begin{cases} \dfrac{f_{ir}}{f_{i\beta}} = 1 & phase\ \beta\ exists \\ \dfrac{f_{ir}}{f_{i\beta}} < 1 & phase\ \beta\ disappears \end{cases} \quad 12$$

The K value of component i in phase β with respect to that in the reference phase r is defined as the ratio of the fugacity coefficient, as follows

$$K_{i,\beta r} = \frac{\varphi_{ir}}{\varphi_{i\beta}} = \frac{x_{i\beta}}{x_{ir}} \frac{f_{ir}}{f_{i\beta}} = \frac{x_{i\beta}}{x_{ir}} \exp(-\ln \frac{f_{i\beta}}{f_{ir}}) \quad i = 1,\ldots,N_C; \beta = 1,\ldots,N_P \tag{13}$$

We introduce a variable θ to quantify the stability of phase β as

$$\theta_\beta = \ln \frac{f_{ir}}{f_{i\beta}}, \beta = 1,\ldots,N_P \tag{14}$$

Therefore, the concentration of component i in phase β is

$$x_{i\beta} = K_{i,\beta r} x_{ir} e^{\theta_\beta} \quad i = 1,\ldots,N_C; \beta = 1,\ldots N_P; \beta \neq r \tag{15}$$

Moreover, Equation 10 can be rewritten as

$$\alpha_\beta \theta_\beta = 0, \beta = 1,\ldots N_P; \beta \neq r \tag{16}$$

The total number of moles of component i can be expressed as

$$\alpha_r x_{ir} + \sum_{\substack{\beta=1 \\ \beta \neq r}}^{\pi} \alpha_\beta x_{i\beta} = z_i \quad i = 1,\ldots,N_C \tag{17}$$

By combining the above equations, we can obtain that

$$x_{ir} = \frac{z_i}{1 + \sum_{\substack{\beta=1 \\ \beta \neq r}}^{\pi} \alpha_\beta (K_{i,\beta r} e^{\theta_\beta} - 1)} \quad i = 1,\ldots,N_C \tag{18}$$

Moreover, the total concentration of component i among all phases should be 1, as follows

$$\sum_{i=1}^{C} x_{i\beta} = 1, \beta = 1,\ldots,N_P \tag{19}$$

We then define the objective functions for each component as

$$D_{i\beta} = x_{i\beta}[1 + \sum_{\substack{j=1 \\ j \neq r}}^{\pi} \alpha_j (K_{i,jr} e^{\theta_j} - 1)] - z_i K_{i,\beta r} e^{\theta_\beta} = 0 \quad i = 1,\ldots,N_C; \beta = 1,\ldots,N_P; \beta \neq r \tag{20}$$

$$E_\beta = \sum_{i=1}^{C} \frac{z_i (K_{i,\beta r} e^{\theta_\beta} - 1)}{1 + \sum_{\substack{j=1 \\ j \neq r}}^{\pi} \alpha_j (K_{i,jr} e^{\theta_j} - 1)} = 0 \quad \beta = 1,\ldots,N_P \tag{21}$$

$$F_\beta = \frac{\alpha_\beta \theta_\beta}{\alpha_\beta + \theta_\beta} = 0 \; \beta = 1,\ldots,N_P \tag{22}$$

Therefore, to minimize the Gibbs energy G^* is to minimize D, E and F simultaneously. The minimization of G^* is essentially an optimization process. By finding the global minima of the objective functions, we can get the phase behaviors of the multiphase system. The parameters required for the flash calculation, including the binary interaction factors, are from (Pan and Oldenburg 2016).

Equation of state and fugacity models

As shown in the previous section, the calculation of the Gibbs energy requires the calculation of the fugacity of the component, which is achieved by the reformulation of an equation of state. In MSFLOW_CO2, Soave-Redlich-Kwong equation of state (SRK-EOS) is used for the calculation of the density as well as fugacity of the vapor hydrocarbon and the liquid hydrocarbon phase. The fugacity of the vapor hydrocarbon and the liquid hydrocarbon phase is shown in the two equations below.

$$\ln\frac{f_i^o}{x_i P} = \frac{b_i}{b}(Z-1) - \ln\left(Z - \frac{bP^o}{RT}\right) + \frac{a}{2\sqrt{2}bRT}\left(\frac{2\sum_{j=1}^{N_C} x_j a_{ij}}{a} - \frac{b_i}{b}\right)\ln\left(\frac{Z+\left(1-\sqrt{2}\right)\frac{bP}{RT}}{Z+\left(1+\sqrt{2}\right)\frac{bP}{RT}}\right) \quad 23$$

$$\ln\frac{f_i^g}{y_i P} = \frac{b_i}{b}(Z-1) - \ln\left(Z - \frac{bP^o}{RT}\right) + \frac{a}{2\sqrt{2}bRT}\left(\frac{2\sum_{j=1}^{N_C} y_j a_{ij}}{a} - \frac{b_i}{b}\right)\ln\left(\frac{Z+\left(1-\sqrt{2}\right)\frac{bP}{RT}}{Z+\left(1+\sqrt{2}\right)\frac{bP}{RT}}\right) \quad 24$$

In the above equation, the parameter a is defined as

$$a = \sum_{i=1}^{N_C}\sum_{j=1}^{N_C} x_i x_j a_{ij} \quad 25$$

a_{ij} is defined as

$$a_{ij} = \left(1-k_{ij}\right)\sqrt{\alpha_i a_i \alpha_j a_j} \quad 26$$

Where k_{ij} is the interaction parameter. a_i and α_i is defined as

$$a_i = 0.42747\frac{R^2 T_{C_i}^2}{P_{C_i}} \quad 27$$

Where T_{C_i} and P_{C_i} is the critical temperature and critical pressure of component i respectively.

$$\alpha_i = \left[1 + S_i^*\left(1-\sqrt{T_{r_i}}\right)\right]^2 \quad 28$$

Where

$$S_i^* = 0.48508 + 1.55151\omega_i - 0.15613\omega_i^2 \quad 29$$

The reduced temperature and pressure is defined as

$$T_{r_i} = \frac{T}{T_{C_i}} \quad 30$$

$$P_{r_i} = \frac{P}{P_{C_i}} \tag{31}$$

In the above equation, ω_i is the acentric parameter of component i

$$b = \sum_{i=1}^{N_C} x_i b_i \tag{32}$$

$$b_i = 0.08664 \frac{RT_{C_i}}{P_{C_i}} \tag{33}$$

In SRK-EOS, the compressibility factor Z is expressed as a cubic function, as below.

$$f(Z) = Z^3 - Z^2 + \left(A - B - B^2\right)Z - A \cdot B = 0 \tag{34}$$

In the above equation,

$$A = \frac{aP}{(RT)^2} \tag{35}$$

$$B = \frac{bP}{RT} \tag{36}$$

Equation 34 is solved analytically. For the three solved compressibility factors, the largest factor and the smallest factor is assigned to the gas phase and the liquid phase respectively.

The aqueous (water) phase properties are calculated based on Shock and Helgeson's (Shock and Helgeson 1988) approach. The chemical potential μ_{iAq} of the ith solute component (non-water component) in the water phase is calculated as

$$\frac{\mu_{iAq}}{RT} = \frac{\bar{g}_i^*}{RT_0} - \int_{T_0}^{T} \frac{\bar{h}_i^*}{RT^2} dT + \int_{P_0}^{P} \frac{\bar{v}_i^*}{RT} dP + \ln a_{iAq} \tag{37}$$

In the above equation, T_0 and P_0 is the standard temperature and pressure respectively. $\bar{g}_i^*$, $\bar{h}_i^*$ and $\bar{v}_i^*$ is the partial molar Gibbs energy, partial molar enthalpy and partial molar volume of a hypothetical solution, respectively. The detailed formulation of $\bar{g}_i^*$, $\bar{h}_i^*$ and $\bar{v}_i^*$ can be found in (Shock and Helgeson 1988). The chemical potential of water component in the water phase is calculated as

$$\frac{\mu_{wAq}}{RT} = \frac{g_{w_0,pure}}{RT_0} - \int_{T_0}^{T} \frac{h_{w,pure}}{RT^2} dT + \int_{P_0}^{P} \frac{v_{w,pure}}{RT} dP + \ln a_{wAq} \tag{38}$$

Where the subscript 'pure' refers to the pure water phase. The details of the implementation of water fugacity can be found in (Bromley 1973; Jager et al. 2003).

We use Newton's method to minimize Equation 20, 21 and 22, as follows.

$$\left[\frac{\partial \Psi_l}{\partial X_j}\right]_p \left\{\Delta X_j\right\}_{p+1} = -\left\{\Psi_l\right\}_p \tag{39}$$

In the above equation, Ψ is the objective function, X is the primary variable and $[\partial\Psi_l/\partial X_j]_p$ is the Jacobian matrix. The initial guess of the equilibrium ratio for the hydrocarbon component in oil and gas phase K_i^0 can be estimated by Wilson's equation, as

$$K_i^0 = \frac{p_{ci}}{p} \exp\left(5.37\left(1+\omega_i\right)\left(1-\frac{T_{ci}}{T}\right)\right) \quad 40$$

The initial guess of the equilibrium ratio of water component in the oil and the gas phase. Moreover, the solubility of the hydrocarbon components in the aqueous phase is set to be 0.

Mechanical properties

The mechanical properties have impacts on the permeability as well as the porosity of the formation rock. In general, the porosity and permeability can be expressed as the function of the pressure, temperature and mean stress, as

$$\phi = \phi\left(P, T, \sigma_m\right) \quad 41$$

$$K = K\left(P, T, \sigma_m\right) \quad 42$$

MSFLOW_CO2 has implemented several correlations of the permeability and porosity, from literature (Rutqvist et al. 2002; Taronet al. 2009; Wang et al. 2016). Moreover, MSFLOW_CO2 allows the users to input a table of permeability and porosity with respect to the primary variables. One example of the correlations is as follows(Wang et al. 2017; Wang et al. 2017). The porosity of the rock can be calculated as

$$\phi = \phi_0\left(1 + c_p\left(P - P_{ref}\right) + 3\beta_T\left(T - T_{ref}\right)\right) \quad 43$$

In the above equation, c_p and β_T is the compressibility and the thermal expansion coefficient, respectively. P_{ref} is a reference pressure, while T_{ref} is a reference temperature. ϕ_0 and ϕ is the initial porosity and the transient porosity of the rock, respectively.

Based on the calculated porosity, the permeability can be calculated by the Carman-Kozeny equation (Carman 1956; Kruczek 2014) as

$$K = K_0\left(\frac{1-\phi_0}{1-\phi}\right)^3\left(\frac{\phi}{\phi_0}\right)^3 \quad 44$$

The pore diameter changes as the stress condition varies. The change of the pore diameter results in the variation of the capillary pressure of the multiphase system. In MSFLOW_CO2, the capillary pressure is correlated with the permeability and porosity as follows (Leverett 1941)

$$P_c = P_{c0}\sqrt{\left(K/\phi\right)_0} \,/\, \sqrt{\left(K/\phi\right)} \quad 45$$

Where P_{c0} and P_c is the initial and the transient capillary pressure, respectively. Moreover, the mechanical impact on the volume of the grid block is quantified via the volumetric strain ε_V as

$$V = V_0\left(1 - \varepsilon_V\right) \quad 46$$

Where V_0 and V is the initial and the transient volume of the grid block, respectively.

Governing equations and numerical approach

Governing equations

Derived from the conservation law of mass and energy, the governing equations of the thermal-hydraulic simulation module in MSFLOW_CO2 describes the fluid and heat transport in the porous media of the

reservoir. For a compositional system consisting of N_C components, the mass/energy conservation equation for component k is as follows

$$\frac{\partial M^k}{\partial t} = \nabla \cdot \vec{F}^k + q^k \quad 47$$

In the above equation, the term M is the accumulation term for mass or energy. $\vec{F}$ is the flux term. t is the time term and q is the sink/source term. k could refer to an aqueous (water) component, a hydrocarbon component or an energy 'component'. In MSFLOW_CO2, k =1 refers to the aqueous (water) component. k = 2,.., N_C denote hydrocarbon components. k = N_C +1 denotes the internal energy. For aqueous and hydrocarbon components, the accumulation term is calculated as

$$M^k = \phi \sum_\beta S_\beta \rho_\beta x_\beta^k, \quad \beta = L, G, A, \quad k = 1,.., N_C \quad 48$$

Where ϕ is the porosity. β is the phase index. G refers to the gas (vapor) hydrocarbon phase; L refers to the liquid hydrocarbon phase and A refers to the aqueous phase. S_β and ρ_β is the saturation and density of phase β respectively. x_β^k is the mass fraction of component k inside phase β. Since the solubility of hydrocarbon in the aqueous phase is very low, in this work we set

$$x_A^k = 0, \quad k = 2,.., N_C \quad 49$$

For the energy 'component',

$$M^{N_C+2} = (1-\phi) C_R \rho_R T + \phi \sum_\beta S_\beta \rho_\beta U_\beta \quad 50$$

where C_R and ρ_R is the specific heat and density of the rock, respectively. U_β is the internal energy of phase β. T is the temperature of the system.

$$\vec{F}^k = \sum_\beta X_\beta^k \vec{F}_\beta \quad 51$$

In Equation 47, the flux term $\vec{F}^k$ is calculated as

$$\vec{F}^k = \sum_\beta \vec{F}_\beta x_\beta^k, \quad k = 1,.., N_C \quad 52$$

In the above equation, x_β^k is the mass fraction of component k inside phase β. The phase flux $\vec{F}_\beta$ is calculated by the multiphase Darcy's law, as shown in Equation 53, where K_a is the apparent permeability of the rock. $K_{r\beta}$ is the relative permeability of phase β, μ_β is the viscosity of β, and $\vec{g}$ is the gravity vector.

$$\vec{F}_\beta = -K_a \frac{K_{r\beta}\rho_\beta}{\mu_\beta}\left(\nabla P_\beta - \rho_\beta \vec{g}\right) \quad 53$$

For the liquid and aqueous phase, K_a is identical to the absolute permeability of the rock K_∞. For the gas phase, $K_a = K_\infty(1+b/p)$, where b is the Klinkenberg parameter, which can be calculated from the work of (Wang et al. 2019). The energy flux has heat conduction and convection as

$$\vec{F}^{N_C+1} = -k_t \nabla T + \sum_\beta h_\beta \vec{F}_\beta \quad 54$$

where k_t is thermal conductivity and h_β is the specific enthalpy of phase β.

The mechanical simulation module of MSFLOW_CO2 is based on mean stress method, as discussed in (Wang et al., 2016). In MSFLOW_CO2, the formation rock is assumed to be a linear poro-thermo-elastic material.

$$\bar{\bar{\tau}} = 2G_S\bar{\bar{\varepsilon}} + \lambda_L(\varepsilon_{xx} + \varepsilon_{yy} + \varepsilon_{zz})\bar{\bar{I}} \quad 55$$

where $\bar{\bar{\tau}}$ is the stress tensor, $\bar{\bar{\varepsilon}}$ is the strain tensor, and $\bar{\bar{I}}$ is a unit tensor. G_S is the shear modulus and λ_L is the Lame's coefficient. ε_{ii}, $k = x, y, z$ is the diagonal terms of the strain tensor.

Equation 55 was extended to non-isothermal materials by Nowacki (2013) and Norris (1992). Moreover, McTigue (1986) brought out the poro-thermo-elastic version of the above equation, as shown below

$$\sigma_{kk} - \left[\alpha P + 3\beta_T K_B\left(T - T_{ref}\right)\right] = \lambda_L\varepsilon_v + 2G\varepsilon_{kk}, \quad k = x, y, z \quad 56$$

where σ_{ii}, $k = x, y, z$ is the diagonal terms of the stress tensor. In Equation 56, β_T and K_B is the thermal expansion coefficient and the bulk modulus respectively. ε_v is the volumetric strain, which is defined as shown in Equation 57.

$$\varepsilon_v = \varepsilon_{xx} + \varepsilon_{yy} + \varepsilon_{zz} \quad 57$$

By rearranging Equation 56, we can get

$$\sigma_m - \alpha P - 3\beta_T K_B\left(T - T_{ref}\right) = \left(\lambda + \frac{2}{3}G_S\right)\varepsilon_v \quad 58$$

in which

$$\sigma_m = \frac{\sigma_{xx} + \sigma_{yy} + \sigma_{zz}}{3} \quad 59$$

is the mean stress.

Meanwhile, the conservation of momentum for the poro-thermo-elastic process can be described by Navier's equation (Eslami et al., 2013), as follow

$$\alpha\nabla P + 3\beta_T K_B\nabla T + \left(\lambda_L + G_S\right)\nabla\left(\nabla\cdot\vec{u}\right) + G_S\nabla^2\vec{u} + \vec{F}_b = 0 \quad 60$$

In the above equation, $\vec{u}$ and $\vec{F}_b$ is the displacement vector and body force respectively. By implementing divergence operations to Equation 60, we can get

$$\alpha\nabla^2 P + 3\beta_T K_B\nabla^2 T + \left(\lambda_L + 2G_S\right)\nabla^2\left(\nabla\cdot\vec{u}\right) + \nabla\cdot\vec{F}_b = 0 \quad 61$$

Moreover, we have the following relationship between the displacement vector and the volumetric strain

$$\nabla\cdot\vec{u} = \varepsilon_v \quad 62$$

By combing Equation 58 and Equation 62 with Equation 61 and rearranging them, we can get the following governing equation for the mechanical simulation,

$$\frac{3(1-\nu)}{(1+\nu)}\nabla^2\sigma_m + \nabla\cdot\vec{F} = \frac{2(1-2\nu)}{(1+\nu)}\left(\alpha\nabla^2 P + 3\beta_T K_B\nabla^2 T\right) \quad 63$$

The relationship among the mechanical modulus is as follows.

$$E = 2G_S\left(1+\nu\right) \quad 64$$

$$E = 3K_B\left(1-2\nu\right) \quad 65$$

$$\lambda_L = \frac{2\nu G_S}{1-2\nu} \tag{66}$$

Numerical approach

In MSFLOW_CO2, all the governing equations are solved by integrated finite difference (IFD) method (Narasimhan & Witherspoon, 1976a). Similar to finite volume method, integrated finite difference method divides the computational domain into numerous grid blocks. After being integrated over grid blocks, the governing equations are converted to accumulation terms on each grid blocks and flux terms on each pair of neighboring grid blocks using the Gaussian divergence theorem. The details of the IFD method used in MSFLOW_CO2 are as follows.

Firstly, integrating Equation 47 over the volume of the nth grid block V_n yields

$$\frac{\partial}{\partial t}\int_{V_n} M^k dV = \int_{\Gamma_n} \vec{F}^k \cdot n d\Gamma + \int_{V_n} q^k dV \tag{67}$$

Where n is the normal vector and Γ is the area. The accumulation term can be then expressed as

$$\int_{V_n} M^k dV = M_n^k V_n \tag{68}$$

In the above equation, M_n^k is the discrete accumulation term of component k on grid block n.

Meanwhile, the flux term can be express as

$$\int_{\Gamma_n} \vec{F}^k \cdot n d\Gamma = \sum_m A_{nm} \vec{F}_{nm}^k \tag{69}$$

Where m loops through all the neighboring grid blocks of grid block n. A_{nm} and $\vec{F}_{nm}^k$ is the area and flux term of component k between grid block m and grid block n, respectively. The time derivative is approximated by the first-order finite difference scheme. Therefore, Equation 67 becomes

$$\left[M_n^k\right]^{l+1} - \left[M_n^k\right]^l - \frac{\Delta t}{V_n}\left[\sum_m A_{nm} F_{nm}^k + V_n q_n^k\right] = 0 \tag{70}$$

where Δt is the time step length and l is time level. By rearranging the terms, the above equation can be expressed in the residual vector form as

$$\mathbf{R}\left(\mathbf{x}^{l+1}\right) = 0 \tag{71}$$

Where $\mathbf{R}$ is the residual vector form and $\mathbf{x}^{l+1}$ is the primary variable vector at time level l+1. The above equation is a nonlinear equation and is solved iteratively by the Newton-Raphson method. A conceptual model of the IFD method is shown in Figure 1. MSFLOW_CO2 is fully implicit and adopts upwind weighting scheme to calculate the flux term.

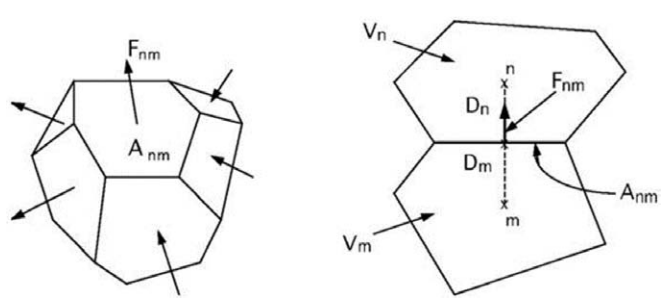

Figure 1—Conceptual model of integral finite difference method (Narasimhan and Witherspoon 1976b; Pruess 1985).

The Newton-Raphson method has been widely used in solving the nonlinear equations arising in scientific computing. The basic idea of the Newton-Raphson method is to use the gradient of the equation to calculate the searching direction of the iteration. The gradient of a vector equation is expressed by the Jacobian matrix. The formulation of the Newton-Raphson method is as below.

$$\mathbf{J} \cdot \Delta \mathbf{x} = -\mathbf{R}(\mathbf{x}) \tag{72}$$

In the above equation, **J** is the Jacobian matrix and $\Delta\mathbf{x}$ is the update the primary variable of each iteration. The Jacobian matrix of a vector equation with N unknowns is defined as follows

$$\mathbf{J} = \begin{bmatrix} \frac{\partial \mathbf{R}}{\partial x_1} & \cdots & \frac{\partial \mathbf{R}}{\partial x_N} \end{bmatrix} = \begin{bmatrix} \frac{\partial R_1}{\partial x_1} & \cdots & \frac{\partial R_1}{\partial x_n} \\ \vdots & \ddots & \vdots \\ \frac{\partial R_n}{\partial x_1} & \cdots & \frac{\partial R_n}{\partial x_n} \end{bmatrix} \tag{73}$$

In MSFLOW_CO2, the partial derivatives are calculated by the numerical derivative. Until convergence, the above equation is iteratively constructed. Within each equation, the above equation is solved by a multiscale linear solver (Hajibeygi and Jenny 2009). More details of the Newton-Raphson method used in MSFLOW_CO2 can be found in (Wang et al. 2015).

Performance of flash calculation

In this section, we present the validation as well as the results of the flash calculation module.

Validation

We first present a seven-component case and compare it with experimental data. The feed mole fraction of the seven-component acid gas system is shown in Table 1. The feed contains H_2S, making it acid gas. We calculate the variation of gas-liquid equilibrium ratio at 338.71K and compare the results with experimental data (Yarborough 1972). The comparison is shown in Figure 2. According to comparison, our proposed flash calculation module matches well with experimental data.

Table 1—Feed mole fraction of a seven-component acid gas system.

Component	Feed mole fraction (%)
CH_4	77.43
C_2H_6	5.74
C_3H_8	2.99
C_5H_{12}	4.66
C_7H_{16}	3.59
$C_{10}H_{22}$	2.63
H_2S	2.96

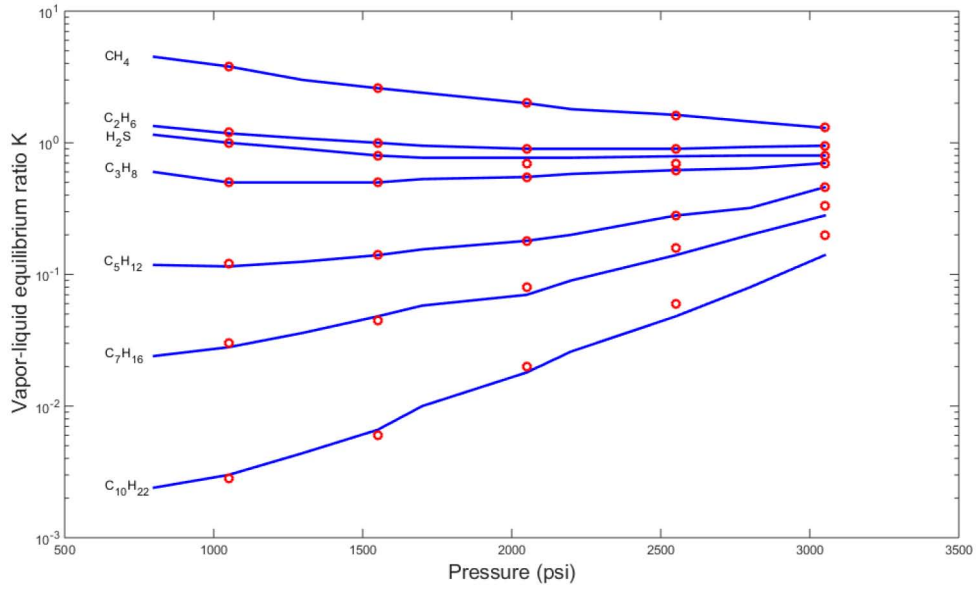

Figure 2—Comparison with laboratory measured gas-liquid equilibrium factor Kgo. at 338.71K.

Flash calculation for three phase systems

In this session, we present the results of the flash calculation module. We run two three- component three-phase cases. The first case is a ternary mixture of CO_2, water and nonane (n-C_9H_{20}). Figure 3 shows the mole fraction of the aqueous phase at 333 K and 30 MPa. The distribution of the mole fracture of the aqueous phase is almost proportional to the water component fraction. The second case is a ternary mixture of a ternary mixture of methane, water and nonane (n-C_9H_{20}). Figure 4 shows the distribution of the mole fraction of the liquid hydrocarbon phase at 333 K and 30 MPa. According to Figure 4, our flash calculation module is able to capture the transition between the gas and the liquid hydrocarbon phase. Based on the validation and the numerical results, it can be concluded that our flash calculation module is able to handle complex multi-phase systems.

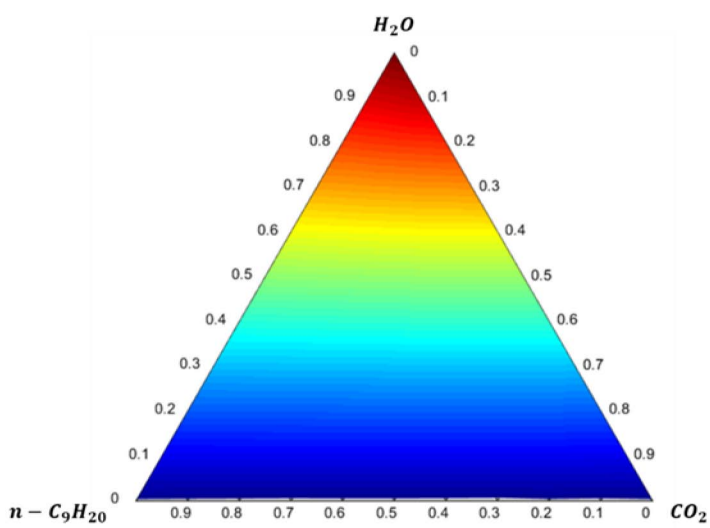

Figure 3—Mole fraction of aqueous phase of the CO2/n-C9H20/H2O mixture at 333 K and 30 MPa.

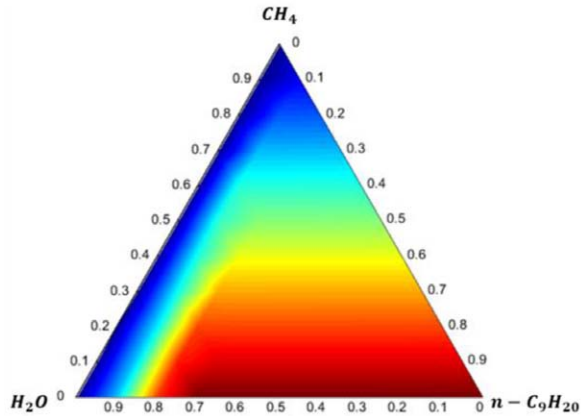

Figure 4—Mole fraction of liquid hydrocarbon phase of the CH4/n-C9H20/H2O mixture at 333 K and 30 MPa.

Deep learning based proxy flash calculation

Overview

We aim to accerelate the flash calculation of compositional simulation by proxy flash calculation. We use deep-learning based stochastic training technique to develop the proxy simulator. We have trained a neural network using fully connected layers, which has an input layer, an output layer, and four hidden layers. Within each layer, there are several neurons elements. All neurons belong to two neighboring layers are fully connected with each other, as shown in Figure 5. In the fully connected layers, each neuron has its weight, including a kernel value and a bias value. During the training process, the algorithm adaptively tunes the weight and send the weight to an activation function, as shown in Figure 6. The summation of the weighted values of all neurons gives the predicted output. The norm of the difference between the input value and the predicted output is defined as the loss function. To minimize the loss function, Adam algorithm is used as the optimizer. The algorithm of SDG is as follows. Firstly, all input samples in the training set are divided into N_B groups, each of which is called a 'mini-batch.' Starting from an initial parameter w and learning rate η, SGD randomly shuffle the samples in the training set and loops through all mini-batch to conduct gradient descent optimization as follows

$$w = w - \eta \nabla Q_i(w), i = 1,..,N_B \tag{74}$$

In the above equation, Q is the loss function. The above process is repeated until the number of iterations reaches pre-defined epochs.

Network structure

In this work, we have implemented a two-step neural network for the proxy flash calculation. The first step, namely phase classification, consists of a fully connected neural network, the purpose of which is to classify the phase condition of the problem. The input dimension of the network is N_C+2. The output dimension is seven, since there are seven possible combination of phases. In between the input and output layer are four hidden layer whose dimension is 64, 64, 64 and 64 respectively, as shown in the left of Figure 7. The input data consists of the pressure, temperature as well as feed concentration (mole fraction of each component), as shown in Equation 75. The output data consists of the tags for each phase condition, as shown in Equation 76 and Table 2.

$$X = \left[P, T, Z_1, ..., Z_{N_c}\right]^T \tag{75}$$

$$Y_1 = \left[I_1, I_2, I_3, I_4, I_5, I_6, I_7\right]^T \tag{76}$$

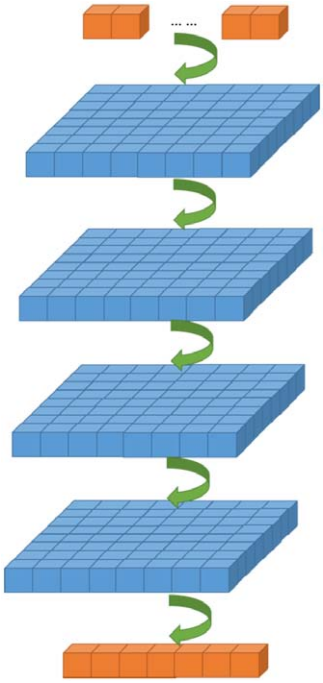

Figure 5—The structure of the artificial neural network.

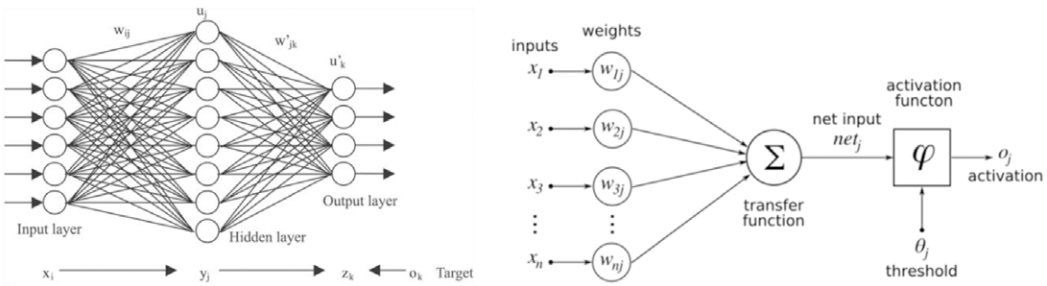

Figure 6—Conceptual model of the fully connected layer and its neurons.

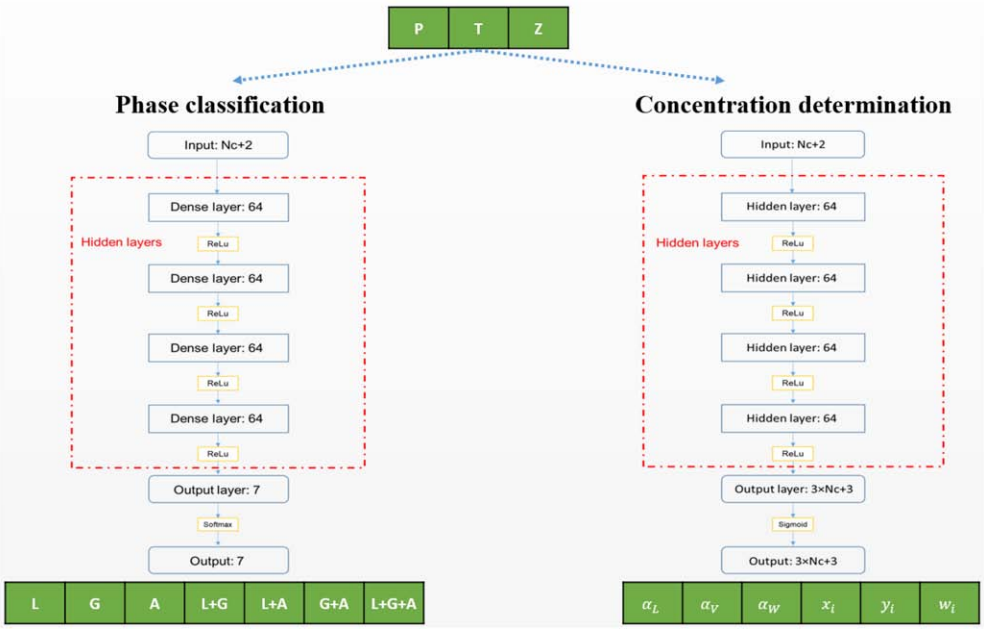

Figure 7—Structure of the fully connected network.

Table 2—Summary of the possible phase combinations for the classification training step.

Classification	Phase Combination
I_1	L
I_2	G
I_3	A
I_4	L+G
I_5	L+A
I_6	G+A
I_7	L+G+A

For the hidden layers we use ReLU function as the activation function, which is defined as

$$\mathrm{ReLU}(x)=\begin{cases}0 & \text{for} \quad x<0\\ x & \text{for} \quad x\geq 0\end{cases} \tag{77}$$

For the output layer the softmax function is chosen as the activation function, defined as

$$\mathrm{softmax}(x)_j=\frac{e^{x_j}}{\sum_{k=1}^{K}e^{x_k}} \tag{78}$$

The loss function is chosen as the cross-entropy function.

$$\mathrm{sigmoid}(x)=\frac{1}{1+e^{-x}} \tag{79}$$

The training data contains 500,000 data sets, of which 100,000 data sets are used as testing data. Each data set contains the input data and the output data.. The physical meanings of the input data are shown in Table 3

$$Y_2=\left[L,V,W,x_1,\ldots,x_{N_c\text{-}1},y_1,\ldots,y_{N_c\text{-}1},w_1,\ldots,w_{N_c\text{-}1}\right]^T \tag{80}$$

In the above equation, L, V and W is the mole fraction of liquid, vapor and aqueous phase respectively. The model is trained with 140 epochs (iterations). Within each iteration, 128 training samples are grouped as a mini-batch. We measure the mean max absolute error (MMAE), mean absolute percentage (MAPE) and mean absolute error (MAE) of the testing results. The three metrics are listed in Table 4, according to which the average accuracy of our proxy simulator is above 97%.

Table 3—Input parameters of the proxy calculation module.

Name	Physical Meaning and Unit
P	Pressure (MPa)
T	Temperature (°C)
Z	Feed (Mole concentration) (dimensionless)

Table 4—Summary of errors of the predicted results under different metrics

	Phase Classification	Concentration Determination	Overall Error	Overall Accuracy
Feed component	Mean Absolute Percentage Error	Mean Absolute Percentage Error	Mean Absolute Percentage Error	Mean Absolute Percentage Accuracy
C1+CO2+N2	0.02%	0.82%	0.84%	99.16%
C1+C2+C3+CO2	0.01%	0.65%	0.66%	99.34%
C1+C2+C4+C7	0.06%	1.63%	1.69%	98.31%
C1+C2+C3+C4+C5	0.07%	1.86%	1.93%	98.07%
C1+C2+C10+CO2+N2+H20	0.11%	2.02%	2.13%	97.87%
C1+C2+C3+C7+C9+C10+CO2+H20	0.11%	2.87%	2.98%	97.02%

Simulation of Cold CO2 injection

In this case, we present a cold CO_2 injection study. Cold CO_2 is injected at a rate of 0.3kg/s into a 100m by 100m reservoir for 1 year. One production well is producing at a constant bottom hole pressure of 16.2 MPa. The initial temperature of the reservoir is 85 °C. The conceptual model of this case is shown in Figure 9. The three-phase relative permeability is calculated using the Brooks-Corey model (Delshad & Pope 1989). The initial distribution of component is shown in Table 5 and Figure 10. The rest input parameters are listed in Table 6. We run three cases, in which the injection temperature (temperature of CO_2 when it arrives at the formation) is 20 °C, 40 °C and 60 °C respectively. The length and width of the domain is 100m*100m. The domain is discretized uniformly into 50*50 grid blocks.

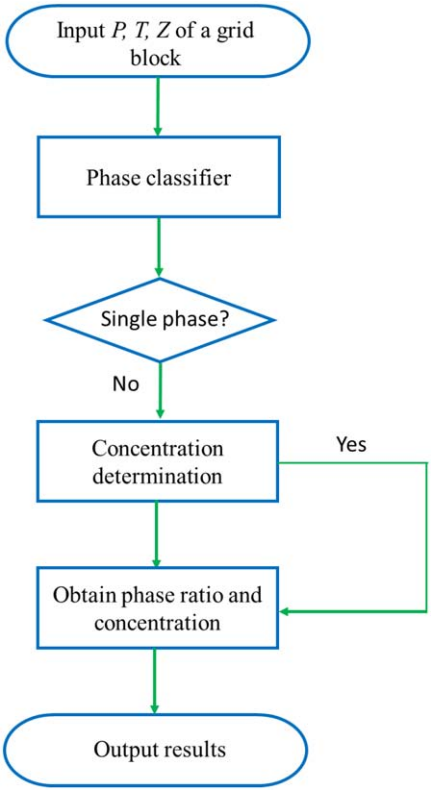

Figure 8—Flowchart of the proxy flash calculation preconditioner in a reservoir simulator.

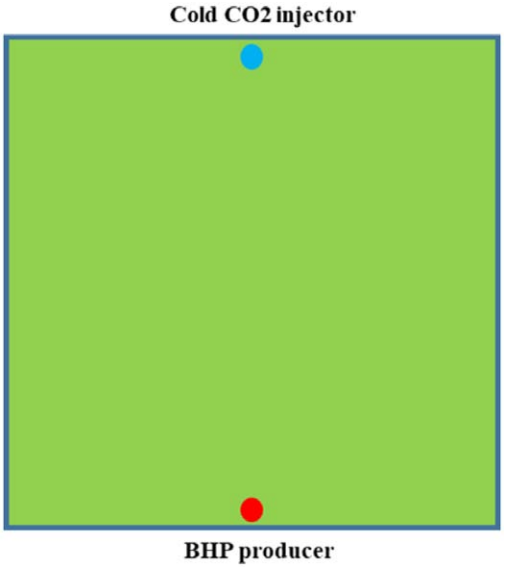

Figure 9—Conceptual model of the cold CO_2 injection case.

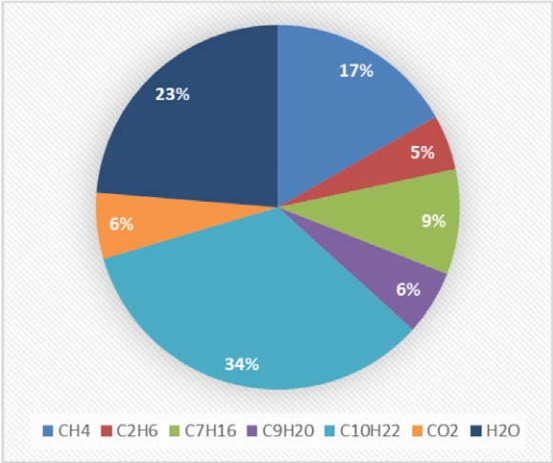

Figure 10—The fraction of initial concentration of the for cold CO_2 injection case.

Table 5—Initial distribution of component for cold CO_2 injection case.

Component	Formula	Mole fraction
Methane	CH_4	0.16736
Ethane	C_2H_6	0.04885
n-Heptane	C_7H_{16}	0.09334
n-Nonane	C_9H_{20}	0.05751
n-Decane	$C_{10}H_{22}$	0.33736
Carbon Dioxide	CO_2	0.05854
Water	H_2O	0.23704

Table 6—Input parameters for cold CO_2 injection case

Property	Value	Unit
Young's modulus	26	GPa
Poisson's ratio	0.25	dimensionless
Rock permeability	1	md
Rock porosity	0.2	dimensionless
Biot's coefficient	1.0	dimensionless
Grid block length	4	m
Injection temperature	50	°C
Initial temperature	85	°C
Initial pressure	35.2	MPa
Production pressure	16.2	MPa
Initial mean stress	80.6	MPa
Residual gas saturation (S_{gr})	0.1	dimensionless
Residual oil saturation (S_{or})	0.1	dimensionless
Residual water saturation (S_{wr})	0.1	dimensionless

The distribution of gas phase saturation and temperature after 1 year of injection is shown in Figure 11 and Figure 12 respectively. According to Figure 11, the gas phase saturation increases near the injector. Therefore, this is immiscible flooding. Moreover, the gas saturation decreases in certain region near the

saturation front. This is because of pressure impact propagates faster than saturation impact. The buildup of pressure decreases the gas saturation in the region near the saturation front.

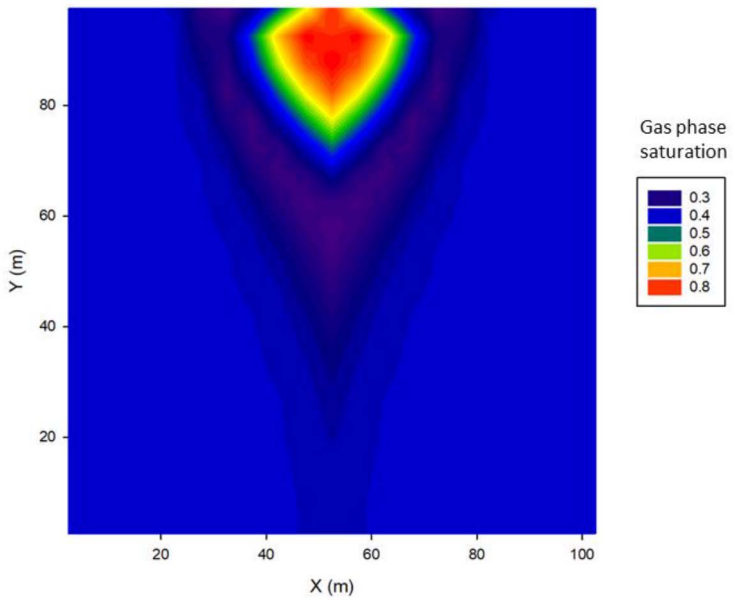

Figure 11—Gas phase saturation distribution after one year of injection (injection temperature = 60 °C).

According to Figure 12, the temperature in the vicinity the producer slightly decreases. The reduction of the temperature is because the energy of the system is consumed by the expansion of the in-situ fluids, known as the Joule-Thomson effect. From this phenomenon, we can conclude that our simulator is capable of capturing many aspects of the complex behaviors of the multiphysical system. The variation of scaled permeability (transient permeability to initial permeability) at the injector with respect to time is shown in Figure 13, according to which the injected cold CO_2 effectively increases the injectivity near the injector. When the injection temperature decreases from 60 °C to 20 °C, the eventual increase of the permeability increases from 170% to 280%. Based on this observation, it can be concluded that cold CO_2 injection can be adopted improve the EOR performance of unconventional reservoirs.

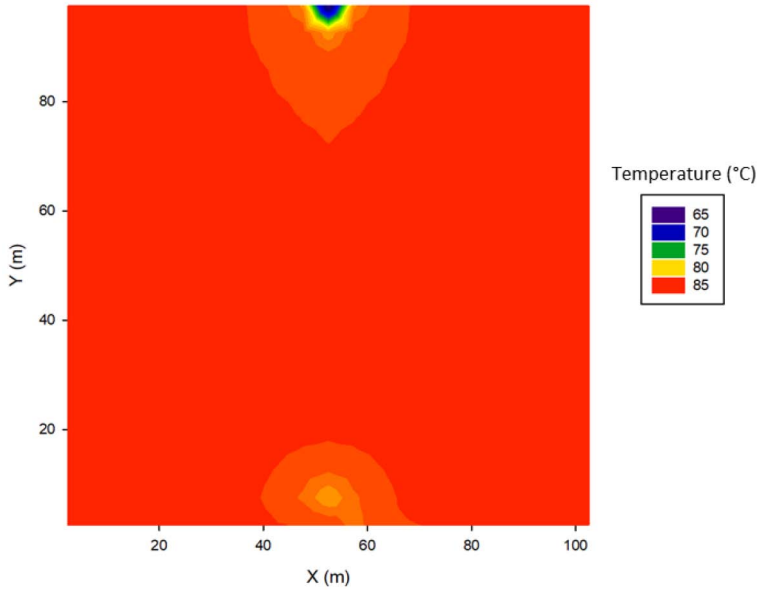

Figure 12—Temperature distribution after one year of injection (injection temperature = 60 °C).

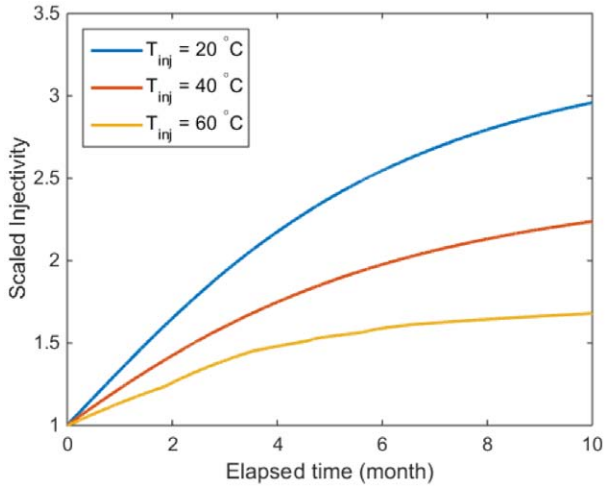

Figure 13—Variation of scaled permeability at the injector with respect to time.

We have implemented the deep-learning based flash calculator into our simulator MSFLOW_CO2. We have conducted several case studies to investigate the performance of the deep learning based compositional simulator. In this chapter, all numerical cases are executed by an Intel i7- 6700 processor with 3.40 GHz.

We first compare the cold CO_2 injection case presented in Chapter 7.05. We test cases with a different number of grid blocks. The comparison of the CPU time with 25*25, 50*50, and 100*100 grid blocks with and without the deep-learning based preconditioner is shown in Figure 14. The comparison shows that the CPU time has been effectively reduced by 30% to 40% by the deep learning based preconditioner.

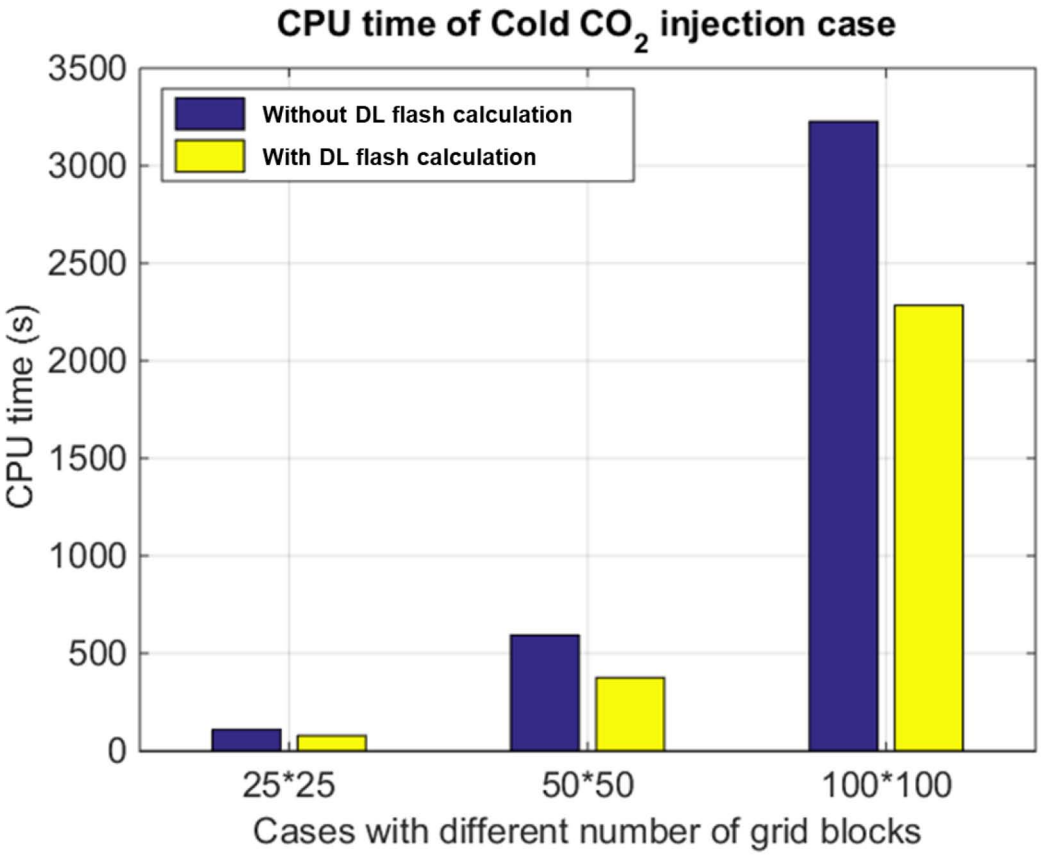

Figure 14—Comparison of the CPU time of the cold CO_2 injection cased with and without the deep- learning based flash calculation.

Summary and Conclusions

We have developed a comprehensive non-isothermal compositional simulator, named as MSFLOW_CO2, to simulate CO2-EOR processes. The simulator is based on the Integrated Finite Difference (IFD) method, which is able to simulate multiphysical flow and transport processes in reservoirs using an unstructured grid.

We have implemented a fully couple thermal-hydraulic-mechanical framework in MSFLOW_CO2 to simulate the multiphysical processes during CO2-EOR. The hydraulic-mechanical module of MSFLOW_CO2 has been verified against analytical solutions with sufficient accuracy. The mean stress method used in this simulator is able to capture the poro-elastic effect during the recovery of petroleum reservoirs. Moreover, the thermal-hydraulic module of MSLOW_CO2 has been benchmarked with a commercial simulator. The results yielded by the two simulators show a good match. Therefore, the accuracy of the multiphysical simulation framework of MSFLOW_CO2 is validated.

To simulate the complex phase behaviors in the REV, we have developed a novel flash calculation module based on minimization of the Gibbs energy method. We have benchmarked the flash calculation module with respect to experimental results. The minimization of the Gibbs energy method shows the flexibility in capturing the phase transition during CO_2 flooding. Moreover, this method can be potentially applied to simulate even more complex systems, for instance, systems with four or more phases.

Based on the developed simulator, we have studied the impact of cold CO_2 injection on the production performance of unconventional reservoirs. Such impact is ignored by existing commercial simulators. We discovered that, cold CO_2 injection effectively increases the injectivity of unconventional reservoirs.

At last, we also developed a data-based proxy flash calculator to speed up the time-consuming flash calculation. With the implementation of the proxy calculator, the CPU time of the simulation of cold CO_2 injection case has been effectively reduced by 30%. This work is among the first trials in this area.

Acknowledgements

The author would like to thank Energi Simulation for their kind support.

Reference

Al-Marhoun, M. A., & Osman, E. A. (2002). Using Artificial Neural Networks to Develop New PVT Correlations for Saudi Crude Oils. In Abu Dhabi International Petroleum Exhibition and Conference. Society of Petroleum Engineers. 10.2118/78592-MS

Ballard, A. L. (2002). A non-ideal hydrate solid solution model for a multi-phase equilibria program. *Colorado School of Mines*. Retrieved from https://dspace.library.colostate.edu/bitstream/handle/11124/78793/T05590.pdf

Ballard, A. L., & Sloan, E. D. (2004). The next generation of hydrate prediction: Part III. Gibbs energy minimization formalism. *Fluid Phase Equilibria*, **218**(1), 15–31. 10.1016/J.FLUID.2003.08.005

Bhargava, V., Fateen, S. E. K., & Bonilla-Petriciolet, A. (2013). Cuckoo Search: A new nature-inspired optimization method for phase equilibrium calculations. *Fluid Phase Equilibria*, **337**, 191–200. 10.1016/J.FLUID.2012.09.018

Bonilla-Petriciolet, A., & Segovia-Hernández, J. G. (2010). A comparative study of particle swarm optimization and its variants for phase stability and equilibrium calculations in multicomponent reactive and non-reactive systems. *Fluid Phase Equilibria*, **289**(2), 110–121. 10.1016/J.FLUID.2009.11.008

Bromley, L. A. (1973). Thermodynamic properties of strong electrolytes in aqueous solutions. *AIChE Journal*, **19**(2), 313–320. 10.1002/aic.690190216

Carman, P. C. (1956). Flow of gases through porous media. Academic press.

Cheung, A., Adjiman, C. S., Kolar, P., & Ishikawa, T. (2002). Global optimization for clusters of flexible molecules—solvent-solute interaction energy calculations. *Fluid Phase Equilibria*, **194–197**, 169–183. 10.1016/S0378-3812(01)00780-4

Computer Modelling Group LTD. (2010). CMG | Software Solutions. Retrieved from https://www.cmgl.ca/software

Delshad, M., & Pope, G. (1989). Comparison of the three-phase oil relative permeability models. *Transport in Porous Media*, **4**(1), 59–83. 10.1007/BF00134742

Di, Y., Zhang, Y., & Wu;Yu-Shu. (2015). Gibbs 自由能最小化法计算二氧化碳-烃-水系统相平衡.. *Acta Petrolei Sinica*, **36**(5), 593–599. Retrieved from http://www.cqvip.com/qk/95667x/201505/665024208.html

Eslami, M., Hetnarski, R., Ignaczak, J., Noda, N., & Sumi, N. (2013). Theory of elasticity and thermal stresses. New York: Springer. Retrieved from http://link.springer.com/content/pdf/10.1007/978-94-007-6356-2.pdf

Gaganis, V., & Varotsis, N. (2012). Machine Learning Methods to Speed up Compositional Reservoir Simulation. In SPE Europec/EAGE Annual Conference. *Society of Petroleum Engineers*. 10.2118/154505-MS

Gharbi, R. B., & Elsharkawy, A. M. (1997). Neural Network Model for Estimating The PVT Properties of Middle East Crude Oils. In Middle East Oil Show and Conference. *Society of Petroleum Engineers*. 10.2118/37695-MS

Grigg, R. B., & Schechter, D. S. (1997). State of the Industry in CO2 Floods. In SPE Annual Technical Conference and Exhibition. *Society of Petroleum Engineers*. 10.2118/38849-MS

Hajibeygi, H., & Jenny, P. (2009). Multiscale finite-volume method for parabolic problems arising from compressible multiphase flow in porous media. *Journal of Computational Physics*, **228**(14), 5129–5147. 10.1016/J.JCP.2009.04.017

Hoffman, E. J. (1968). Flash calculations for petroleum fractions. *Chemical Engineering Science*, **23**(9), 957–964. 10.1016/0009-2509(68)87081-2

Jager, M. D., Ballard, A. L., & Sloan, E. D. (2003). The next generation of hydrate prediction: II. Dedicated aqueous phase fugacity model for hydrate prediction. *Fluid Phase Equilibria*, **211**(1), 85–107. 10.1016/S0378-3812(03)00155-9

Kaya, E., Zarrouk, S. J., & O'Sullivan, M. J. (2011). Reinjection in geothermal fields: A review of worldwide experience. *Renewable and Sustainable Energy Reviews*, **15**(1), 47–68. 10.1016/j.rser.2010.07.032

Kruczek, B. (2014). Carman-Kozeny Equation. In Encyclopedia of Membranes (pp. 1–3). Berlin, Heidelberg: Springer Berlin Heidelberg. 10.1007/978-3-642-40872-4_1995-1

LeCun, Y., Bengio, Y., & Hinton, G. (2015). Deep learning. *Nature*, **521**(7553), 436–444. 10.1038/nature14539

Leibovici, C. F., & Neoschil, J. (1992). A new look at the Rachford-Rice equation. *Fluid Phase Equilibria*, **14**, 303–308.

Leibovici, C. F., & Neoschil, J. (1995). A solution of Rachford-Rice equations for multiphase systems. *Fluid Phase Equilibria*, **112**(2), 217–221. 10.1016/0378-3812(95)02797-I

Leverett, M. C. (1941). Capillary Behavior in Porous Solids. *Transactions of the AIME*, **142**(01), 152–169. 10.2118/941152-G

Ma, Z. (2013). Phase Behaviors of Reservoir Fluids with Capillary Effect Using Particle Swarm Optimization. *King Abdullah University of Science of Technology*.

Manrique, E. J., Thomas, C. P., Ravikiran, R., Izadi Kamouei, M., Lantz, M., Romero, J. L., & Alvarado, V. (2010). EOR: Current Status and Opportunities. In SPE Improved Oil Recovery Symposium. *Society of Petroleum Engineers*. 10.2118/130113-MS

McTigue, D. F. (1986). Thermoelastic response of fluid-saturated porous rock. *Journal of Geophysical Research*, **91**(B9), 9533. 10.1029/JB091iB09p09533

Michelsen, M. L. (1982a). The isothermal flash problem. Part I. Stability. *Fluid Phase Equilibria*, **9**(1), 119. 10.1016/0378-3812(82)85001-2

Michelsen, M. L. (1982b). The isothermal flash problem. Part II. Phase-split calculation. *Fluid Phase Equilibria*, **9**(1), 21–40. 10.1016/0378-3812(82)85002-4

Narasimhan, T. N., & Witherspoon, P. A. (1976a). An integrated finite difference method for analyzing fluid flow in porous media. *Water Resources Research*, **12**(1), 57–64. 10.1029/WR012i001p00057

Narasimhan, T. N., & Witherspoon, P. A. (1976b). An integrated finite difference method for analyzing fluid flow in porous media. *Water Resources Research*, **12**(1), 57–64. 10.1029/WR012i001p00057

Nichita, D. V., Gomez, S., & Luna, E. (2002). Multiphase equilibria calculation by direct minimization of Gibbs free energy with a global optimization method. *Computers & Chemical Engineering*, **26**(12), 1703–1724. 10.1016/S0098-1354(02)00144-8

Norris, A. (1992). On the correspondence between poroelasticity and thermoelasticity. *Journal of Applied Physics*, **71**(3), 1138. 10.1063/1.351278

Nowacki, W. (2013). Thermoelasticity (2nd ed.). Elmsford, New York: Pergamon Press Inc.

Okuno, R., Johns, R., & Sepehrnoori, K. (2010a). A New Algorithm for Rachford-Rice for Multiphase Compositional Simulation. *SPE Journal*, **15**(02), 313–325. 10.2118/117752-PA

Okuno, R., Johns, R., & Sepehrnoori, K. (2010b). A New Algorithm for Rachford-Rice for Multiphase Compositional Simulation. *SPE Journal*, **15**(02), 313–325. 10.2118/117752-PA

Okuno, R., Johns, R. T., & Sepehrnoori, K. (2010c). Three-Phase Flash in Compositional Simulation Using a Reduced Method. *SPE Journal*, **15**(03), 689–703. 10.2118/125226-PA

Pan, L., & Oldenburg, C. M. (2016). TOGA: A TOUGH code for modeling three-phase, multicomponent, and non-isothermal processes involved in CO2-based Enhanced Oil Recovery. Berkeley, CA (United States). 10.2172/1332134

Pruess, K. (1985). A Practical Method for Modeling Fluid and Heat Flow in Fractured Porous Media. *Society of Petroleum Engineers Journal*, **25**(01), 14–26. 10.2118/10509-PA

Rao, D. (2001). Gas Injection EOR- A New Meaning in the New Millennium. *Journal of Canadian Petroleum Technology*, **40**(02). 10.2118/01-02-DAS

Rossi, C. C. R. S., Cardozo-Filho, L., & Guirardello, R. (2009). Gibbs free energy minimization for the calculation of chemical and phase equilibrium using linear programming. *Fluid Phase Equilibria*, **278**(1-2), 117–128. 10.1016/J.FLUID.2009.01.007

Rutqvist, J., Wu, Y.-S., Tsang, C.-F., & Bodvarsson, G. (2002). A modeling approach for analysis of coupled multiphase fluid flow, heat transfer, and deformation in fractured porous rock. *International Journal of Rock Mechanics and Mining Sciences*, **39**(4), 429–442. 10.1016/S1365-1609(02)00022-9

Schlumberger. (2009). INTERSECT High-Resolution Reservoir Simulator.

Shock, E. L., & Helgeson, H. C. (1988). Calculation of the thermodynamic and transport properties of aqueous species at high pressures and temperatures: Correlation algorithms for ionic species and equation of state predictions to 5 kb and 1000°C. *Geochimica et Cosmochimica Acta*, **52**(8), 2009–2036. 10.1016/0016-7037(88)90181-0

Stefansson, V.-dur. (1997). Geothermal reinjection experience. *Geothermics*, **26**(1), 99–139. 10.1016/S0375-6505(96)00035-1

Tang, H., Wang, S., Yin, C., Di, Y., Wu, Y.-S., & Wang, Y. (2019). Fully-Coupled Multi-Physical Simulation with Physics-Based Nonlinearity-Elimination Preconditioned Inexact Newton Method for Enhanced Oil Recovery. *Communications in Computational Physics*, **1**(25), 244–265.

Taron, J., Elsworth, D., & Min, K.-B. (2009). Numerical simulation of thermal-hydrologic-mechanical- chemical processes in deformable, fractured porous media. *International Journal of Rock Mechanics and Mining Sciences*, **46**(5), 842–854. 10.1016/j.ijrmms.2009.01.008

Walton, S., Hassan, O., Morgan, K., & Brown, M. R. (2011). Modified cuckoo search: A new gradient free optimisation algorithm. *Chaos, Solitons & Fractals*, **44**(9), 710–718. 10.1016/J.CHAOS.2011.06.004

Wang, L., Tian, Y., Yu, X., Wang, C., Yao, B., Wang, S., ... Wu, Y.-S. (2017). Advances in improved/enhanced oil recovery technologies for tight and shale reservoirs. *Fuel*, **210**, 425–445. 10.1016/J.FUEL.2017.08.095

Wang, L., Wang, S., Zhang, R., Wang, C., Xiong, Y., Zheng, X., . Rui, Z. (2017). Review of multi-scale and multi-physical simulation technologies for shale and tight gas reservoirs. *Journal of Natural Gas Science and Engineering*, **37**, 560–578. 10.1016/j.jngse.2016.11.051

Wang, S., Huang, Z., Wu, Y.-S., Winterfeld, P. H., & Zerpa, L. E. (2016). A semi-analytical correlation of thermal-hydraulic-mechanical behavior of fractures and its application to modeling reservoir scale cold water injection problems in enhanced geothermal reservoirs. *Geothermics*, **64**, 81–95. 10.1016/j.geothermics.2016.04.005

Wang, S., Lukyanov, A. A., & Wu, Y.-S. (2019). Second-order gas slippage model for the Klinkenberg effect of multicomponent gas at finite Knudsen numbers up to 1. *Fuel*, **235**, 1275–1286. 10.1016/J.FUEL.2018.08.113

Wang, S., Winterfeld, P. H., & Wu, Y.-S. (2015). An Efficient Adaptive Nonlinearity Elimination Preconditioned Inexact Newton Method for Parallel Simulation of Thermal-Hydraulic-Mechanical Processes in Fractured Reservoirs. In SPE Reservoir Simulation Symposium. Society of Petroleum Engineers. 10.2118/173227-MS

YARBOROUGH, L. (1972). Vapor-Liquid Equilibrium Data for Multicomponent Mixtures Containing Hydrocarbon and Nonhydrocarbon Components. *Journal of Chemical and Engineering Data*, **17**(2), 129–133. Retrieved from https://pubs.acs.org/doi/pdf/10.1021/je60053a027

Zhang, H., Bonilla-Petriciolet, A., & Rangaiah, G. P. (2011). A Review on Global Optimization Methods for Phase Equilibrium Modeling and Calculations. *The Open Thermodynamics Journal*, **5**, 71–92.

Zhong, H., Wu, K., Ji, D., & Chen, Z. (2017). Using Least Square Support Vector Machines to Approximate Single Phase Flow. In SPE Europec featured at 79th EAGE Conference and Exhibition. Society of Petroleum Engineers. 10.2118/185881-MS